Eddy Modulation of Air–Sea Interaction and Convection

IVANA CEROVEČKI AND JOHN MARSHALL

Department of Earth, Atmospheric, and Planetary Sciences, Massachusetts Institute of Technology, Cambridge, Massachusetts

(Manuscript received 27 January 2006, in final form 8 January 2007)

ABSTRACT

Eddy modulation of the air–sea interaction and convection that occurs in the process of mode water formation is analyzed in simulations of a baroclinically unstable wind- and buoyancy-driven jet. The watermass transformation analysis of Walin is used to estimate the formation rate of mode water and to characterize the role of eddies in that process. It is found that diabatic eddy heat flux divergences in the mixed layer are comparable in magnitude, but of opposite sign, to the surface air–sea heat flux and largely cancel the direct effect of buoyancy loss to the atmosphere. The calculations suggest that mode water formation estimates based on climatological air–sea heat flux data and outcrops, which do not fully resolve ocean eddies, may neglect a large opposing term in the heat budget and are thus likely to significantly overestimate true formation rates. In Walin's watermass transformation framework, this manifests itself as a sensitivity of formation rate estimates to the averaging period over which the outcrops and air–sea fluxes are subjected. The key processes are described in terms of a transformed Eulerian-mean formalism in which eddy-induced mean flow tends to cancel the Eulerian-mean flow, resulting in weaker residual mean flow, subduction, and mode water formation rates.

1. Introduction

"Mode waters" are thick, broadly distributed, vertically homogeneous, near-surface layers of water. They have been identified in every ocean basin, always on the warm side of a current or front (e.g., Hanawa and Talley 2001). The first identified and most intensively studied is Eighteen Degree Water (EDW) associated with the Gulf Stream Extension in the North Atlantic Ocean (Worthington 1959). EDW is thought to be formed in wintertime convection in the western North Atlantic, just south of the Gulf Stream, in the presence of strong shear with competing effects of vertical and lateral mixing, advection, and stirring working together to set its properties (e.g., Worthington 1959, 1976; Schroeder et al. 1959; Ebbesmeyer and Lindstrom 1986). A characteristic feature of EDW is its low potential vorticity (PV), which tags the water mass and allows it to be mapped far from its source (see McCartney 1982). Although EDW is a historically well-observed property of the subtropical gyre, the relative importance of the different processes that produce this major feature is still debated. Numerical models can capture mode water formation (e.g., Hazeleger and Drijfhout 1998, 1999, 2000; Marsh and New 1996; Paiva and Chassignet 2002). However, there is a considerable disconnect between various estimates of EDW formation rates: whereas up to 15–20 Sv (Sv $\equiv 10^6$ m^3 s^{-1}) of formation are implied by climatological air–sea flux measurements using Walin's (1982) framework (Speer and Tziperman 1992), only 5 Sv have been estimated to be injected seasonally into the subtropical gyre, both from observations using profiling floats (Kwon and Riser 2005) and inferences based on thermocline diapycnal mixing rates. The discrepancy clearly indicates that the relative importance of the various processes contributing to mode water formation and dissipation rates is not yet well understood. However, closing the budget is an important matter since mode waters are the primary water mass that interacts with the atmosphere in key regions of air–sea interaction such as the Gulf Stream and its recirculation.

It is generally accepted that mode waters are formed

Corresponding author address: Ivana Cerovečki, Physical Oceanography Research Division, Scripps Institute of Oceanography, University of California at San Diego, Nierenberg Hall, Room 345, MC 0230, La Jolla, CA 92093-0230.
E-mail: icerovec@ucsd.edu

DOI: 10.1175/2007JPO3545.1

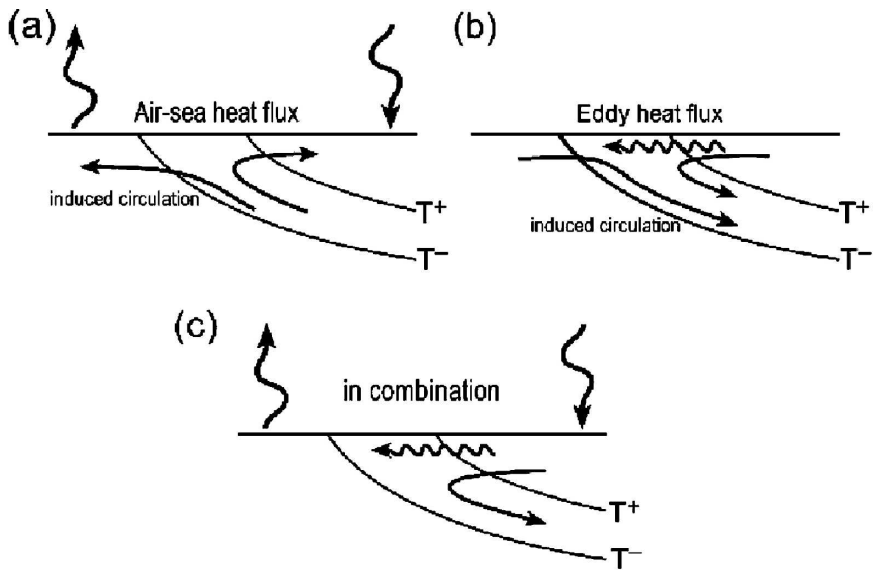

FIG. 1. Illustration of eddy modulation of air–sea interaction in an idealized unstable frontal region with warm water on one side of the front and cold water on the other side, mixed across the front by eddies. Schematic of the (top left) diapycnal volume flow induced by air–sea heat flux, (top right) diapycnal volume flow induced by eddy heat flux, and (bottom) their sum in the case when eddy heat flux exceeds air–sea heat flux. Wiggly arrows indicate the direction of the eddy heat flux.

in the process of winter vertical convection, which is triggered by heat loss from the ocean to the atmosphere, and so can be modulated by, for example, the North Atlantic Oscillation (NAO) (see Marsh and New 1996). However, when analyzing data from the Panulirus station, Jenkins (1982) obtained a poor correlation between local surface air–sea flux and variations in the properties of subtropical mode water. Similarly, Talley and Raymer (1982), analyzing data from the same station, observed that "in fact, the heat flux was nearly out of phase with the Eighteen Degree Water properties." This imperfect correlation between local surface air–sea flux and variations in the properties of subtropical mode water may be an indication that there are processes other than surface heat loss that play an important role in mode water formation.

Since mode waters tend to form adjacent to strong baroclinically unstable fronts, eddy processes may play a central role in mode water formation and dispersal (see Dewar 1986). Indeed, Marshall (1997, hereinafter DM97) showed that mesoscale eddies provide a mechanism to modify the rate at which a water mass is transferred from the surface mixed layer of the ocean into the ocean interior, in particular in regions of strong baroclinic instability. Dong and Kelly (2004) analyzed the importance of ocean advection and heat storage in the heat budget of the Gulf Stream region using a simple three-dimensional thermodynamic model. They found some indication that variations in ocean heat content appear to induce air–sea heat fluxes over the Gulf Stream (their Fig. 13). The authors suggest that advection of anomalies in boundary currents may "precondition" the water column for mode water formation. Kelly (2004) reported similar results for the western North Pacific Ocean and also found that latitudinal variations of heat content and surface flux were negatively correlated.

As an introduction to the processes under consideration in this paper, consider a frontal system with warm water on one side and cold water on the other side, as sketched in Fig. 1. The isopycnals are tilted, so there is both horizontal and vertical shear and the frontal region will be baroclinically unstable, generating eddies that drive the sea surface temperature out of equilibrium with the temperature of the atmosphere above. Since baroclinic eddies stir horizontally, they transport colder water toward the warm side of the front: water on the warmer side becomes colder than the atmosphere above it and gains heat from the atmosphere. Similarly, water on the cold side of the front becomes warmer than the atmosphere above and so loses heat to the atmosphere. Such air–sea heat exchange, if acting alone, would drive diapycnal volume fluxes giving rise to divergent volume flow across the isopycnals, drawing fluid from the interior toward the surface (as sketched in Fig. 1a). However, lateral eddy fluxes directed down

the mean temperature gradient induce a convergent diapycnal volume flow and subduction that opposes the divergent surface flow set up by air–sea heat flux (Fig. 1b). If the eddy heat flux is stronger than the air–sea heat flux, diapycnal flow will be convergent and give rise to subduction, which can carry low-PV fluid formed at the surface into the interior (Fig. 1c). In such a case, mode water properties may be in phase with the eddy heat flux but out of phase with the air–sea heat flux. Thus the volume and properties of mode water might not then be directly slaved to the air–sea flux but also depend on the nature of lateral eddy processes. The flows described in Fig. 1a and discussed above are required to satisfy volume and heat budgets. They may be realized dynamically in many different ways, depending on the detailed nature of the flow and the flow geometry.

Although the significant disconnect between estimates of mode water formation rates in the Gulf Stream region motivated this work, rather then attempting to model mode water formation in any particular ocean basin, instead we analyze an idealized numerical front, as schematically shown in Fig. 1, that becomes unstable and displays mode water formation. Our eddy-resolving model contains key features that are believed to be important in mode water formation: the presence of vigorous eddies adjacent to a strongly sheared baroclinic front, with the resulting formation of low PV water by convective processes triggered by strong air–sea heat exchange and modulated by mesoscale eddies. We address the relative importance of the various processes involved in mode water formation and dissipation, in particular the competing roles of air–sea heat flux and eddy heat flux. We also study the effect of eddy processes in modulating air–sea interaction and convection and, hence, the properties of mode waters. We apply Walin's (1982) water mass formation analysis to both eddy-resolving and non-eddy-resolving "data" from the model and study the difference.

We deliberately choose a very simple geometry for our investigation so as to yield readily interpretable results. The flow geometry adopted is perhaps most relevant to the Antarctic Circumpolar Current and Subantarctic Mode Water formation, but it also illuminates mode water formation in general. One should note, however, that our choice of a channel geometry precludes the following processes: the presence of a background gyral flow with an intense poleward flowing boundary current that can bring surface waters out of equilibrium with the atmosphere, triggering convection and mode water formation; synoptic atmospheric variability, especially the outbreaks of cold air which give rise to wintertime convective mixing due to buoyancy loss from the ocean surface; a seasonal cycle that gives rise to "Stommel's mixed layer demon" (Stommel 1979), which only allows fluid to leave the mixed layer at the end of winter.

Whereas DM97 developed the formalism of the Walin analysis in an eddying ocean and pointed out the importance of eddy buoyancy fluxes to the process of water formation, we present here a detailed case study with eddy-resolved numerical flow fields. DM97 notes that eddy fluxes in the mixed layer include both an advective and a diapycnal component but neglects the diapycnal part of the eddy buoyancy flux in the mixed layer when applying the theory to the Southern Ocean circulation. Here we diagnose both components of eddy buoyancy flux and find that the diapycnal component is large in the mixed layer and that its divergence largely cancels the air–sea heat flux. Our procedure is to first perform the Walin analysis on a model dataset that has sufficient resolution in space and time to capture the eddies. We then "coarse grain" the same dataset before carrying out the same analysis: the difference reveals the eddy effects.

The model used is the Massachusetts Institute of Technology General Circulation Model (MITgcm) (Marshall et al. 1997a,b). The simplicity of the model setup (described in section 2a) allows one to diagnose the heat budget in the upper ocean and separate the individual terms into mean and eddy contributions. The equilibrium state of the flow is described in section 2b. The diagnostic framework of Walin's water mass transformation analysis is briefly outlined and then applied in section 3. Since observational datasets with the necessary spatial and temporal resolution required to represent ocean eddies are rarely available, averaging either in space or time is required to define eddy-related quantities. It is then necessary to account in some way for eddy heat fluxes directed laterally through the mixed layer, as sketched in Fig. 1b. As described in section 4, we suggest a way forward guided by the formalism of the transformed Eulerian mean (TEM). In section 5, the role of the air–sea coupling strength is reviewed and the effect of modifying the coupling strength in our calculations briefly examined. Discussion and conclusions are presented in section 6.

2. Model

a. Model setup

The model used is the MITgcm (Marshall et al. 1997a,b), configured in a pie-shaped sector of the sphere and run hydrostatically. We consider the formation of mode water in the vicinity of a strong and strongly variable jet in a zonally reentrant channel on

the sphere lying between the equator and 50°S.[1] The model has a horizontal resolution of ⅙°. The sector is 10° wide in the zonal direction with periodic boundary conditions imposed at longitudinal boundaries. The model ocean is 4 km deep and has 15 vertical levels of unequal thickness, with a free-slip boundary condition at the equator and a no-slip boundary condition at the polar wall. The simplicity of the geometry allows one to investigate the role played by eddies in zonal-averaged dynamics in terms of both the conventional Eulerian mean and the TEM. Note that with zonally periodic flow reminiscent of the Southern Ocean, our results are also (and perhaps arguably more) relevant to the formation of South Atlantic Mode Water.

A linear equation of state is assumed: $\rho = \rho_0(1 - \alpha_T T)$, where α_T is the thermal expansion coefficient and T is temperature. Isotherms and isopycnals thus coincide. The mixed layer is represented using the "KPP" scheme of Large et al. (1994). Small-scale diffusion of momentum (K^v) and temperature (K^T) are also represented: a Laplacian diffusion in the vertical direction ($K_z^v = 10^{-3}$ and $K_z^T = 10^{-5}$ m^2 s^{-1}) and biharmonic diffusion in the horizontal direction ($K_h^v = 2 \times 10^{11}$ and $K_h^T = 10^{10}$ m^4 s^{-1}).

The flow is forced at the surface by an idealized wind stress and by air–sea heat fluxes. The heat flux $\mathcal{H}$ (W m^{-2}) is determined by relaxing the temperature of the uppermost model layer [of thickness d_1 (here 10 m) and temperature SST] to a specified equilibrium temperature T^* (shown in Fig. 2) on a time scale τ. Thus,

$$\mathcal{H} = \rho c_w \frac{(T^* - \text{SST})d_1}{\tau}. \quad (1)$$

Initally we set τ to 30 days, but sensitivity of our results to this relaxation time is discussed in section 5. Both wind stress and equilibrium temperature are functions of latitude only (Fig. 2.) The wind stress is directed eastward everywhere, becomes very small within 10°S of the equator, and reaches a maximum at 33°S: the Ekman layer transport convergence induces downwelling equatorward of the maximum and Ekman upwelling on the poleward side. The meridional equilibrium temperature gradient is maximum around 20°S and marks the latitude of the mean eastward-flowing jet.

The model was integrated from a state of rest with a horizontally uniform stratification. The flow rapidly became baroclinically unstable. We show model results after 700–800 years of integration, when time-averaged budgets are close to the steady state.

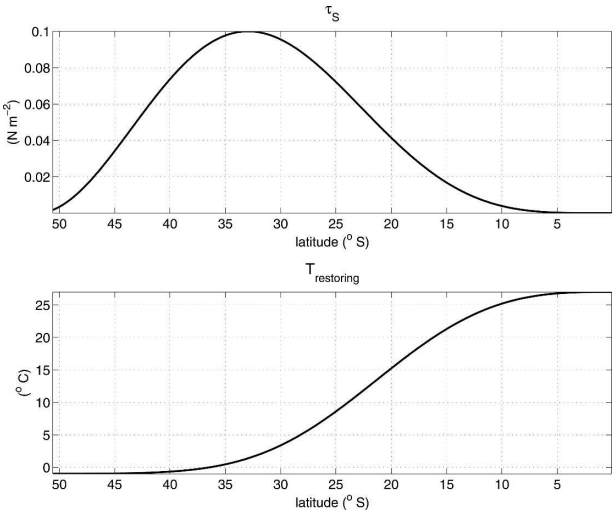

FIG. 2. The wind stress forcing τ_S (N m^{-2}) and the restoring temperature (°C) used to drive the ocean model. The restoring time scale in Eq. (1) is one month in our reference experiment.

b. Phenomenology

A snapshot (daily average) of zonal mean temperature after 750 years of numerical integration (Fig. 3, top) shows widely separated isopycnals between latitudes of 10° and 15°S at depths from 100 to 800 m, indicating the existence of a low-PV pool. The low-PV pool is on the equatorward flank of the core of the eastward jet (Fig. 3, bottom). It is well known that both barotropic and baroclinic flows on the sphere develop jets (e.g., Panetta 1993; Rhines 1994). The present flow exhibits a strong eastward jet centered at 20°S (roughly corresponding to the maximum gradient in T^*) flanked by multiple jet structures on both sides, whose presence is clearly evident both in the zonal mean zonal velocity, shown in Fig. 3, as well as in the instantaneous sea surface temperatures, shown in Fig. 4. Close to the equator, where the wind is weak, eddy processes are not strong, and the fluid column remains rather uniformly stratified. On the poleward flank of our region of focus, surface cooling triggers convection and vertically homogenizes the fluid column over great depth (Fig. 3, top).

Figure 4 shows a horizontal snapshot of sea surface temperature. The zonal extent of the channel is 10° and the domain is periodic (note that three periods are plotted to facilitate visualization of the flow). The strongest eddy activity is confined between latitudes 10° and 30°S and comprises a single eddy between 10° and 15°S. We call this the "mode one" eddy. Poleward of it, smaller

[1] The particular calculation described here was originally designed for studies of the Southern Ocean (Cerovečki et al. 2006, manuscript submitted to *J. Phys. Oceanogr.*).

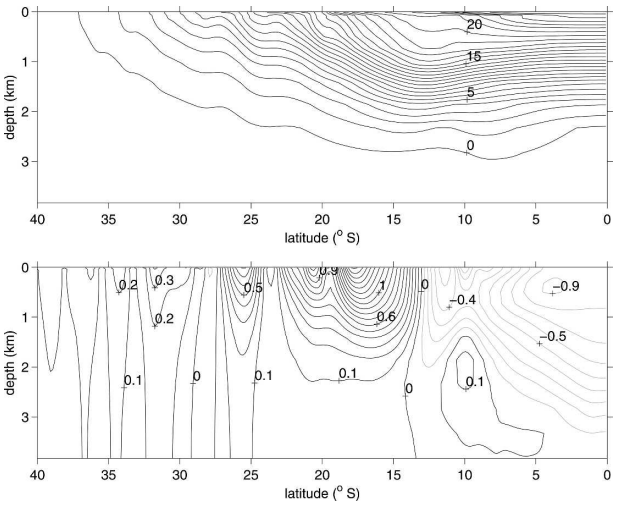

FIG. 3. (top) Instantaneous snapshot of zonal mean temperature (°C). Note the low potential vorticity pool evident in the spreading of isotherms from 21° to 19°C, located between 10° and 15°S latitude at depths from 100 to 800 m. (bottom) Instantaneous snapshot of zonal mean zonal velocity for the same time, after 756 years of integration (m s^{-1}).

scales are evident, but they are less energetic. The dominant and strongly persistent mode one eddy is found just equatorward of the main eastward jet. It is likely that the zonal scale of the eddy is determined by the width of the reentrant channel—initially one observes the zonal scale expanding as energy cascades to larger scales until it becomes as large as the geometry permits.

Reynolds stresses give rise to strong horizontal shear around 15°S. In the critical layer between the eastward and westward flows, the flow wraps up the contours of absolute vorticity so that the mode one eddy develops a Kelvin's cat's eye structure—a lens-shaped region of closed streamlines within which temperature as well as vorticity is nearly uniform. The circulation along these streamlines is counterclockwise. Finescale structures are continuously generated and dissipated. Figure 4 shows that both warm and cold water filaments are formed, with warm filaments being advected poleward and cold filaments equatorward.

Figure 5 shows daily average synoptic maps of sea surface temperature, air–sea fluxes, and mixed layer depth (obtained from the KPP scheme) at two different times separated by 22 days. As noted above, warm water is advected poleward and wrapped around the mode one eddy on its poleward side, thus filling a growing region (centered ~15°S) between the eddy and the jet with warm water. In this manner the equatorward flank of the eastward jet is warmed, making this region prone to convection because the atmosphere above is colder than the surface water. Heat is thus released to the atmosphere (Fig. 5b), and convection results, deepening the mixed layer within the warm water filaments (Fig. 5c). In our model convective events occur in warm water filaments. In reality, of course, convective events can also be triggered by atmospheric variability (e.g., cold air outbreaks over the western North Atlantic and western North Pacific). The sensitivity of the eddy-induced convection to the strength of the air–sea coupling in our simulation is discussed in section 5.

Convection generates low-PV water that will subsequently be shown to feed the low-PV pool. This can be seen in Fig. 6, showing a typical convective event (top panel): patches of low PV are injected into the interior by convection occurring around 16°S. After a major convective event, water restratifies and low-PV fluid spreads equatorward along isopycnals (middle panel), giving rise to a low-PV pool (characterized by small values of negative PV) that lies between the 20° and 21°C isotherm (bottom panel). Note that in both cases (i.e., top and bottom) convection occurs equatorward of the main jet, whose position is indicated by tightly spaced isotherms, placed around $y \approx 20°$S in the top panel and $y \approx 16°$S in the bottom panel. (Note that Fig. 6 is not zonally averaged.)

To more directly document the history of fluid parcels we modeled the evolution of passive tracers in the flow. Figure 7 shows a snapshot of the distribution of passive scalars at the time of a major convective event for five different injected tracers advected over approximately 30 years after release; for each tracer the concentration in the uppermost layer is relaxed to a specified distribution that is sharply peaked in latitude and independent of longitude with a relaxation time of 3 days. Appreciable concentrations are subsequently found below the surface layer only for tracers injected at the latitude corresponding to major convective events (as in release 3, where the concentration is peaked at 16°S latitude). In this case the tracer is mixed down by convective events and thereafter is spread into the ocean interior by eddy processes. The tracer ultimately fills the region of low PV.

We now go on to quantify the formation of mode water in our model and diagnose the processes responsible for it.

3. Diagnostic framework: The "Walin" formalism

a. Background theory

In this section we make use of Walin's (1982) theory of watermass transformation to estimate formation rates of low-PV water in our numerical simulation. Consider, in the spirit of Walin, and using the notation

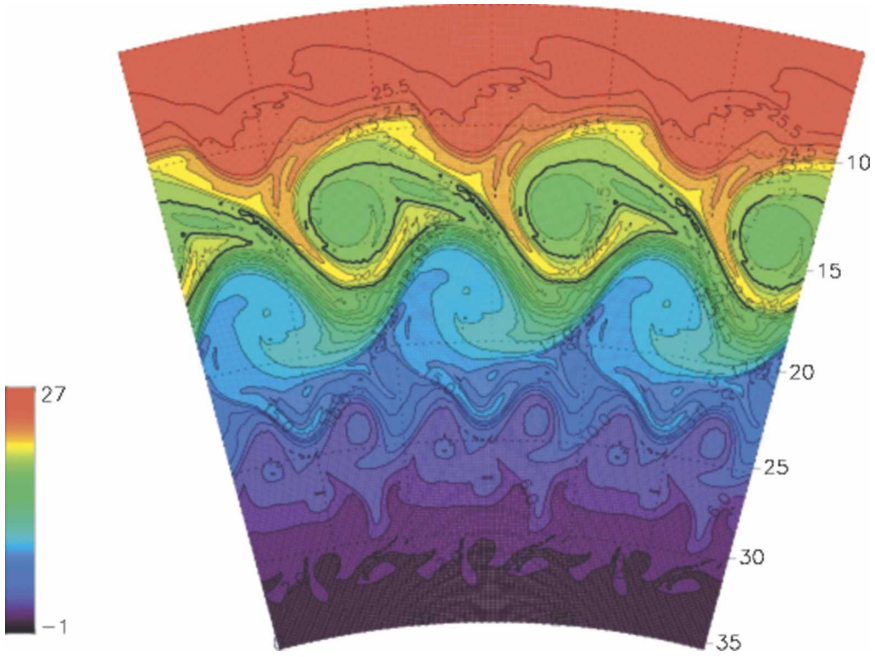

FIG. 4. A snapshot of sea surface temperature (°C); the periodic field is plotted three times in longitude, and only latitudes between 5° and 35°S are shown. The thick line indicates the 22°C isotherm.

of Garrett et al. (1995) and Marshall et al. (1999), the conservation of volume V and density (anomaly) σ for the region $R(\sigma, t)$, sketched in Fig. 8, which extends laterally over the whole ocean basin and terminates at coastal boundaries; it is bounded above by the sea surface, below by a fixed interior Eulerian surface $z = -h(x, y)$, across which we wish to compute the volume flow, and laterally by surfaces of constant density, σ and σ_1. The two isopycnal surfaces that bound the region $R(\sigma, t)$ have areas $\mathcal{A}_\sigma(\sigma, t)$ and $\mathcal{A}_\sigma(\sigma_1, t)$ [see Fig. 2 in Marshall et al. (1999) and Fig. 8 herein]. Here σ_1 is a conveniently chosen reference density taken to be less than σ.

Conservation of the volume V of region $R(\sigma, t)$ can be expressed as

$$\frac{\partial V}{\partial t} = A(\sigma_1, t) - A(\sigma, t) - M(\sigma, t), \tag{2}$$

where $A(\sigma_1, t)$ is the net volume flux through the isopycnal surface labeled σ_1 ($\mathrm{m^3\,s^{-1}}$) and M is the net volume flux across the surface $h(x, y)$ in the density interval from σ_1 to σ, integrated across the ocean basin from one coast to the other. Here A is positive for flow that is directed from lighter to heavier fluid (i.e., poleward) and is defined by

$$A(\sigma, t) = \int\int_{\mathcal{A}_\sigma(\sigma,t)} (\mathbf{u} - \mathbf{u}_\sigma) \cdot \mathbf{n}_\sigma \, d\mathcal{A}, \tag{3}$$

where $\mathbf{u}_\sigma$ is the velocity of an isopycnal surface normal to itself, which is given by

$$\mathbf{u}_\sigma = -\mathbf{n}_\sigma \frac{\partial\sigma/\partial t}{|\nabla\sigma|}, \tag{4}$$

and $\mathbf{n}_\sigma \equiv \nabla\sigma/|\nabla\sigma|$ is a unit vector normal to the isopycnal surface pointing in the direction of maximum density increase.

By using the conservation of density (proportional to buoyancy) written in the form

$$\frac{\partial \sigma}{\partial t} + \nabla \cdot (\mathbf{u}\sigma + \mathbf{N}_\sigma) = 0, \tag{5}$$

where $\mathbf{u}$ is the fluid velocity, $\mathbf{u}\sigma$ is the advective flux of density, and $\mathbf{N}_\sigma$ the nonadvective flux of density, Walin (1982) showed that A can be related to the nonadvective supply of density to the volume $R(\sigma, t)$:

$$A(\sigma, t) = \frac{\partial B(\sigma, t)}{\partial \sigma}, \tag{6}$$

where

$$B = -\int\int\int_{R(\sigma,t)} \nabla \cdot \mathbf{N}_\sigma \, dV. \tag{7}$$

Using the notation of Garrett et al. (1995) and Marshall et al. (1999), we separate B in Eqs. (6) and (7) into "surface" and "interior" contributions to obtain

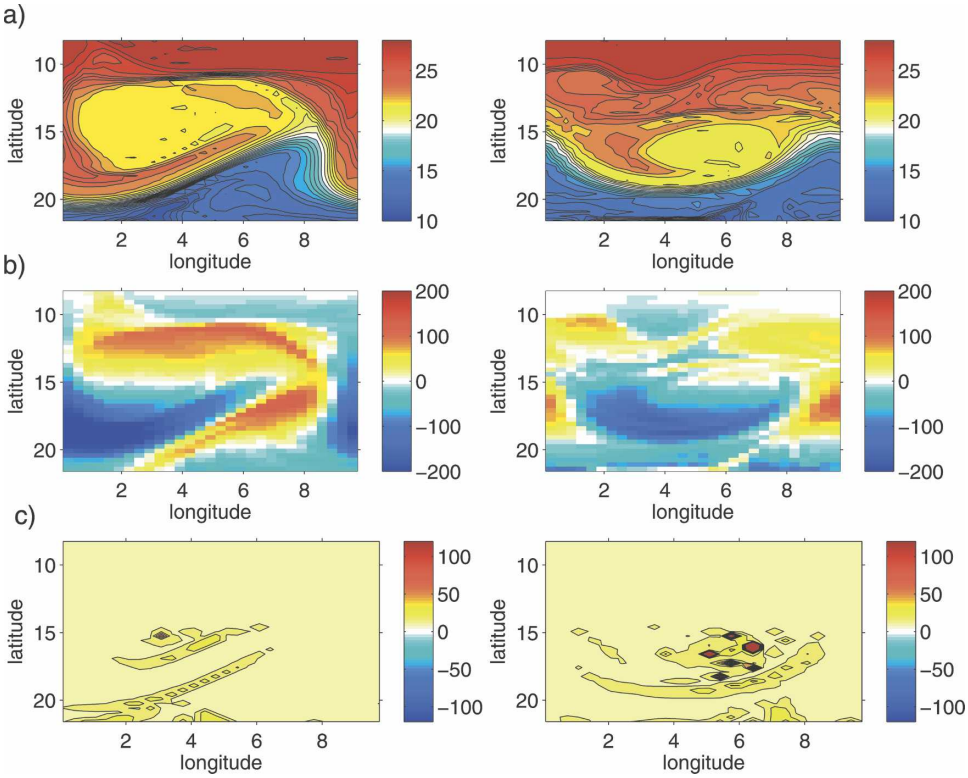

FIG. 5. Synoptic maps of sea surface temperatures (°C) with contour interval 0.5°C, heat flux (W m^{-2}), and mixing layer depth with contour interval 10 m, obtained from the KPP scheme, 22 days apart. Negative heat flux is out of the ocean.

$$A = F - \frac{\partial D}{\partial \sigma}. \tag{8}$$

Here

$$F = \frac{\partial B_S}{\partial \sigma} \tag{9}$$

is the "transformation" associated with air–sea fluxes, and

$$B_S = -\int\int_{\mathcal{A}_S(\sigma,t)} \mathcal{B}_S \, d\mathcal{A} \tag{10}$$

is obtained as an area integral of the air–sea density flux, $\mathcal{B}_S$, through the outcrop window bounded by the reference density σ_1 on one side and σ on the other side (see Fig. 8). The air–sea density flux B_S is directly proportional to the air–sea heat flux (W m^{-2}, positive for ocean gaining heat). The interior contributions comprise the nonadvective (diffusive) supply across interior density surfaces bounding the region $R(\sigma, t)$, which include two lateral isopycnal surfaces with densities σ and σ_1 and the fixed interior Eulerian surface $z = -h(x, y)$, across which we compute the volume flow:

$$D = \int\int \mathbf{N}_\sigma \cdot \mathbf{n}_\sigma \, d\mathcal{A}. \tag{11}$$

The convergence of A gives the rate at which fluid is being added to (or subtracted from) a layer bounded by two adjacent isopycnals and is therefore called the "formation rate," defined by

$$\text{formation rate} \equiv -\frac{\partial A}{\partial \sigma}. \tag{12}$$

For more details see Marshall et al. (1999).

Note that, although time does not explicitly appear, Eq. (8) is an exact expression even in the time-dependent case. Indeed, DM97 points out that the time-mean subduction of a water mass should be evaluated following the meandering surface density outcrops. Garrett and Tandon (1997) have also noted that, in order to accurately estimate A using Eq. (8), it is necessary to follow the instantaneous isopycnals in time. Donners et al. (2005) recently studied water mass transformation and subduction in the South Atlantic by applying the Walin method to numerical model results obtained at eddy-permitting resolution (¼° × ¼°) and point out

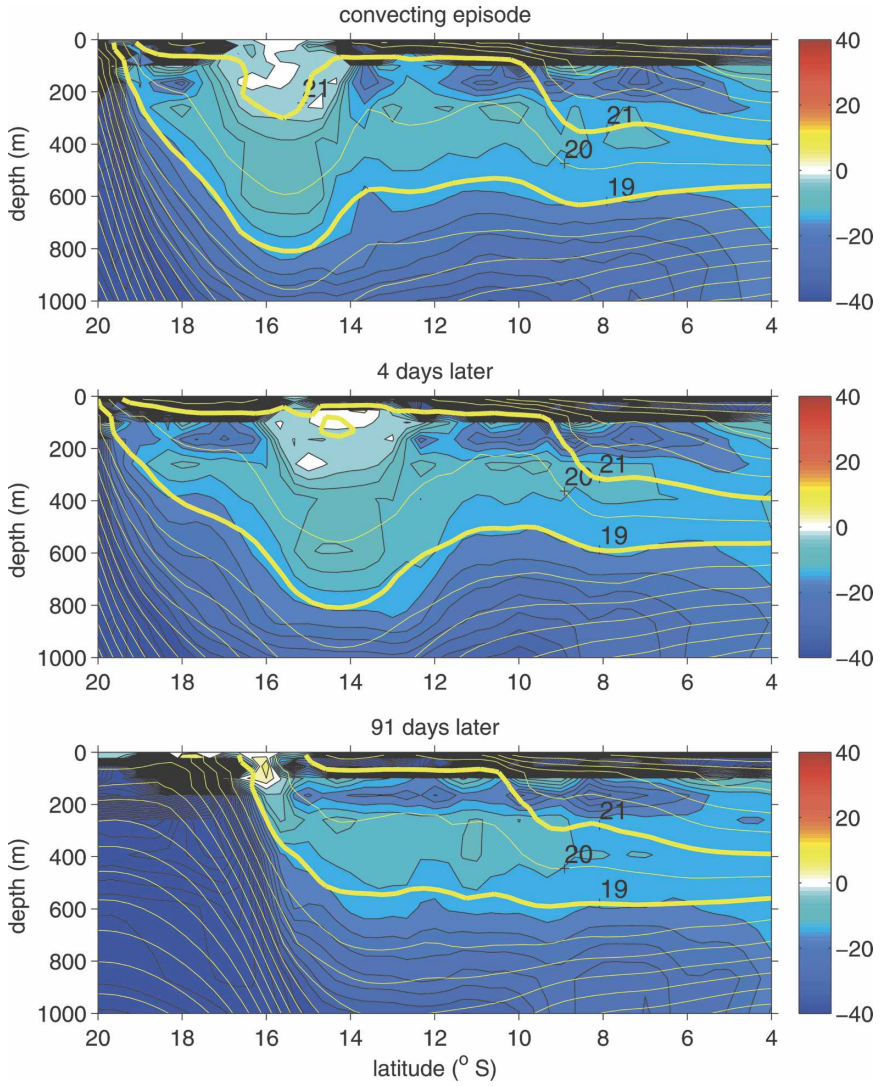

FIG. 6. Snapshot (daily averaged) of Ertel PV obtained as $\overline{\mathrm{PV}} = \overline{\zeta_a \cdot \nabla T}$ [filled color contours; 10^{-8} (°C m^{-1} s^{-1})] and isopycnals (light lines, which coincide with isotherms; °C) at a fixed longitude of 5°. (top) A typical convective episode around 16°S generating low-PV fluid (characterized by small negative and positive values of PV, indicated by light shades). (middle) Snapshot taken four days later (water with lowest PV is now around 14°S, feeding the low-PV pool). (bottom) Low-PV water spreading into the interior, 91 days later.

the importance of eddy processes in this calculation. The importance of following the meandering surface density outcrops is also shown very clearly in our study.

b. *An illustration using "climatological" air–sea fluxes and outcrops*

As an illustration, we first consider a Walin analysis performed using 100 annually averaged model sea surface temperature and air–sea heat flux fields. To estimate transformation rate F due to density flux B_S in Eqs. (9) and (10), we first express the density flux in terms of air–sea heat flux using the relation

$$\mathcal{B}_S = \frac{\alpha}{c_w}\mathcal{H}, \tag{13}$$

where α is the coefficient of thermal expansion of water (taken as a positive constant in our forward integration) and c_w is the heat capacity of water. We use the heat flux $\mathcal{H}$ (W m^{-2}) given by Eq. (1).

The surface distribution of the air–sea heat flux $\mathcal{H}$ is shown in the top panel of Fig. 9 together with the SST averaged over 100 years. If $\mathcal{H} > 0$, then the ocean is warmed; if $\mathcal{H} < 0$ it is cooled. The zonally averaged value of this air–sea heat flux is also plotted against

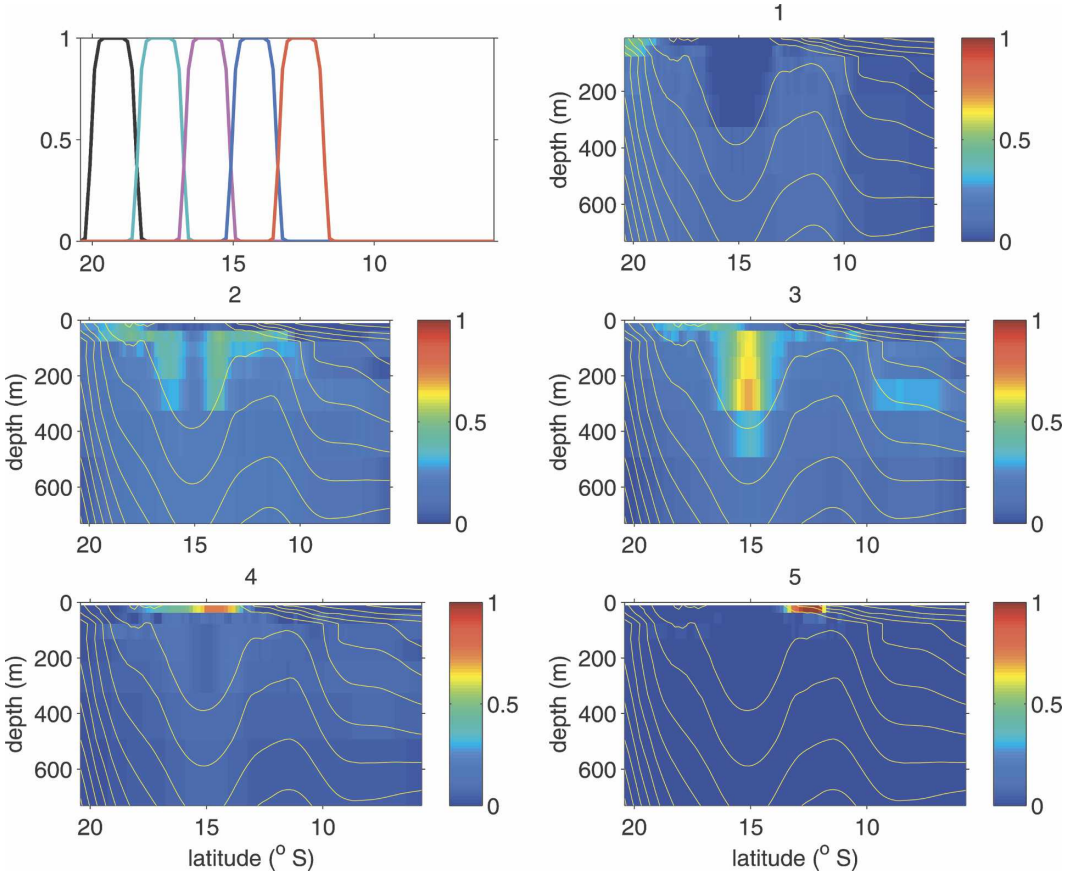

FIG. 7. Meridional distribution from five tracer releases; in each the tracer concentration in the uppermost layer is restored on a 3-day time scale to a specified distribution independent of the zonal direction and meridionally distributed as shown in the upper-left panel (tracer profiles are labeled 1–5, from left to right). Remaining panels show tracer concentration for each release at a longitude $x = 5°$ after 30 years.

temperature in the top panel of Fig. 10. The bottom panel of Fig. 10 shows the diapycnal volume flux A obtained from Eq. (8) using time-mean SST and air–sea flux data, with neglect of interior contribution $\partial D/\partial\sigma$ and expressing the surface density flux using Eqs. (9), (10), (1), and (13): the diapycnal volume flux A implied by air–sea fluxes alone is negative (i.e., directed equatorward) equatorward of 15°S (corresponding to the mean temperature of ~21°C) and positive (i.e., poleward) poleward of this latitude. Hence, just as depicted schematically in Fig. 1a, analysis of air–sea fluxes derived solely from heavily averaged surface heat flux would suggest that fluid is being drawn up toward the surface around 15°S (in the temperature range from ~21° to ~23°C). But is this the correct sense of the diapycnal volume flux in an ocean with strong eddies? One must be cautious when working with data that have the effect of eddies averaged out. Indeed, we will now show that the actual sense of the diapycnal volume flux is very different—and is in fact directly opposite—when account is taken of the role of eddies. To illustrate, we will carry out a Walin analysis following instantaneous outcrops and air–sea density fluxes at sufficiently high resolution in space and time to resolve eddy processes (section 3c). To estimate the significance of the role that eddies play in formation of low PV water, we go on to average these datasets over successively longer time intervals and perform a Walin analysis on increasingly "coarse grained" data (see Fig. 8, right). How sensitive will the implied transformation rates be to the degree of coarse graining?

c. *Application of the Walin formalism to instantaneous isotherms*

We first perform a Walin analysis using Eq. (8) from the output of the model simulation described in section 2a that has sufficient resolution in both space and time to represent eddy processes. We use temperature data sampled each day and calculate the formation rate be-

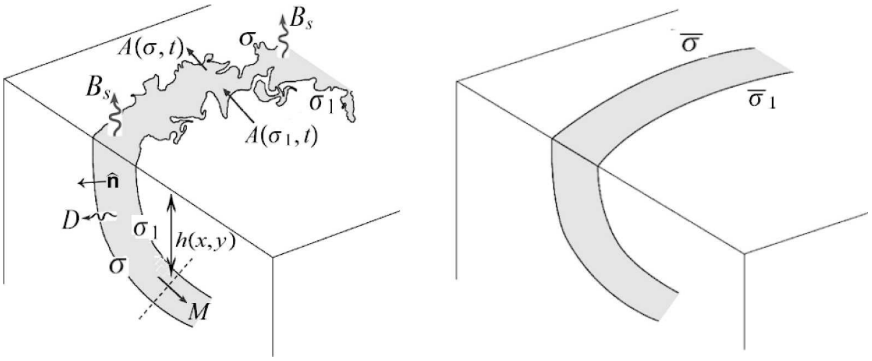

FIG. 8. Schematic showing application of the formalism due to Walin (1982): (left) Sketch of the outcrop in the presence of the eddies. The shaded region $R(\sigma, t)$ is bounded laterally by two outcropping isopycnals with density σ and reference density σ_1 (less than σ), and vertically by the sea surface and a control surface $z = -h(x, y)$. Lateral volume flow $A(\sigma, t)$ across the isopycnals, whose convergence drives net subduction M across the control surface $h(x, y)$ in the ocean interior, is induced by air–sea density flux B_S acting across the sea surface and the interior density flux D acting across the lateral isotherms: $\mathbf{n}_\sigma$ is the unit vector perpendicular to the isopycnals. (right) The corresponding picture after coarse graining, which spatially smooths isopycnals and the outcropping window bounded by $\overline{\sigma}$ and $\overline{\sigma}_1$.

tween the instantaneous isotherms as they move around from day to day.

The nonadvective supply of density, Eq. (11), is computed from N_σ, taking into account the various diffusive terms employed in the model forward run:

$$\mathbf{N}_\sigma = -\left[K_z \frac{\partial \sigma}{\partial z}\mathbf{z} + K_H \nabla_{\mathbf{H}}(\nabla_H^2 \sigma) + K_{\gamma_\sigma}\mathbf{z} \right], \quad (14)$$

where K_z is a vertical diffusion parameter representing both interior mixing by internal wave breaking and enhanced mixing due to convection (see Klinger et al. 1996), K_H is the coefficient of biharmonic horizontal diffusion (used to control grid-scale noise in the tracer equations), and K_{γ_σ} is the "nonlocal term" in the KPP scheme (see Large et al. 1994).

Figure 11 shows the volume flux A (top panel) and the formation rate $\partial A/\partial T$ (bottom panel), both obtained using synoptic SST and air–sea heat flux data.[2] We see a pronounced peak in formation of 2 Sv of water formed in the temperature class centered at 21°C. Comparison of the volume flux estimate obtained by taking both air–sea heat flux and diffusive heat flux into account in Eq. (8), with that based on only air–sea heat flux, shows that the contribution of the diffusive heat flux is very small relative to the air–sea heat flux (Fig. 11). This is encouraging and shows that "numerical" issues, as well as resolved diffusive fluxes, do not play a significant role in setting formation rates in the model.

We see, then, that by using synoptic data we diagnose a very different pattern of A than that given in Fig. 10 and one that indeed implies a formation of mode water in the observed temperature range.

d. Walin analysis using time-averaged air–sea heat flux data

In the previous section we applied the Walin analysis to synoptic data with sufficient resolution in space and time to resolve the eddies, in which case D represents the small-scale diffusive heat flux. However, a dataset with sufficiently fine resolution in space and time to resolve eddies is rarely available, so typically one needs to work with data that have been time averaged at a fixed location. To study how averaging affects the accuracy of formation rate estimates obtained by Walin's (1982) analysis, we time average the temperature model results (those used in section 3c) on the Eulerian grid of the model and use them to calculate outcrop windows and air–sea heat fluxes. Although there is no time-dependent forcing in our model, there is intrinsic time variability due to baroclinic instability. We now compare the results of Walin's analysis obtained using successively more heavily time-averaged data (which smoothes out the temperature field and outcrop windows) with those obtained using synoptic data.

Figure 12 compares estimates of A using Eq. (8) and setting $D = 0$ but retaining the air–sea flux contribution in F via Eqs. (10), (1), and (13), using (i) daily outcrops

[2] For consistency with the literature, especially Marshall et al. (1999), we use density as the independent variable in equations leading to the formation rate estimates. However, since we use a linear equation of state with salinity assumed constant, we present the results of our calculations using temperature as the independent variable.

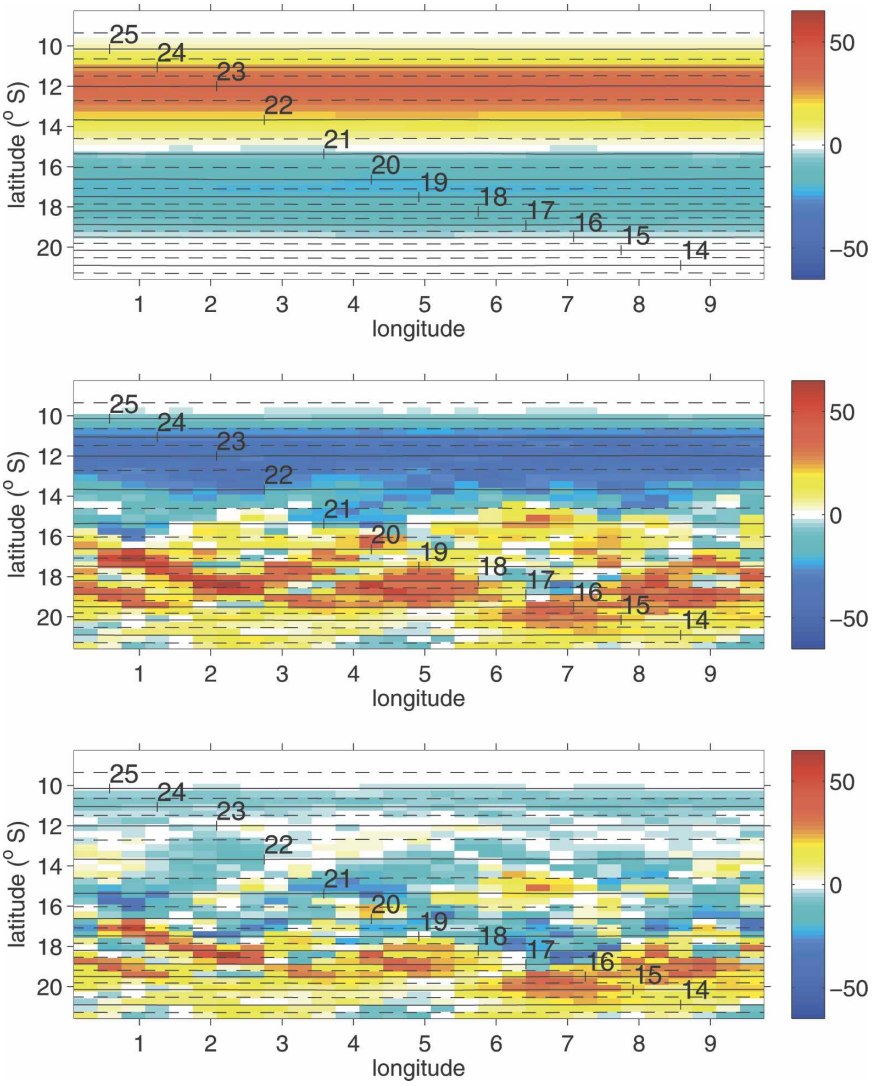

FIG. 9. (top) Air–sea heat flux H, (middle) vertically integrated diapycnal eddy heat flux divergence given by Eq. (16), and (bottom) their sum. Plots are time averaged over 100 years (W m^{-2}). Air–sea fluxes warming the ocean are positive. The zonal average of each panel is shown in Fig. 14. In all panels, black lines are contours of SST time averaged over 100 years.

and air–sea flux data, (ii) monthly averaged data, and (iii) yearly averaged data. As shown in the upper panel of Fig. 12, the dominant process captured in all transformation rate estimates is that the ocean loses heat in the temperature range from ~17° to 21°C and gains heat in the temperature range from ~21° to 25°C. This pattern of air–sea heat flux is induced by the presence of the mode one eddy and is the only heat exchange process represented when using annually averaged air–sea heat flux data and outcrops. In strong contrast, use of daily air–sea heat flux data reveals a much more intense heat exchange confined to a narrow temperature range: a peak in heat loss in the temperature range 21°–23°C corresponding to the low-PV pool. This is the typical temperature range of warm water eddy filaments (seen in Fig. 4), which advect heat poleward and release it to the colder atmosphere above, triggering convection and formation of water of temperature 20.5°–21.5°C (Fig. 12, bottom). This is the process responsible for mode water formation in our zonally periodic flow geometry.[3] In annually averaged data, the filaments of warm water are averaged out, so these data do not capture heat loss to the atmosphere associated with the eddy filaments and they "miss" formation of

[3] Note that in gyre flow, such as the one that includes the Gulf Stream, mode water can be formed in the absence of eddies.

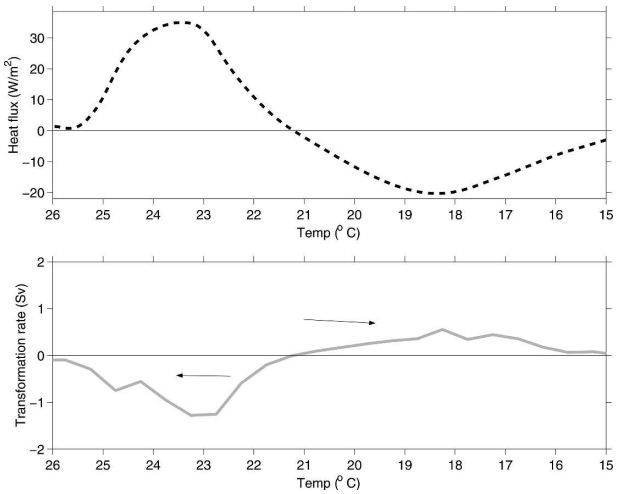

FIG. 10. Results obtained by performing a Walin analysis on 100 years of annually and zonally averaged model SST data. (top) The air–sea heat flux (W m^{-2}) obtained from Eq. (1) using 100 years of annually and zonally averaged model SST data [also shown plotted against latitude in Fig. 9 (top)]. (bottom) The diapycnal volume flux A diagnosed from Eq. (8) with "interior contributions" $\partial D/\partial T$ neglected and with B_s in Eq. (9) determined from the heat flux of the top panel making use of Eqs. (10) and (13).

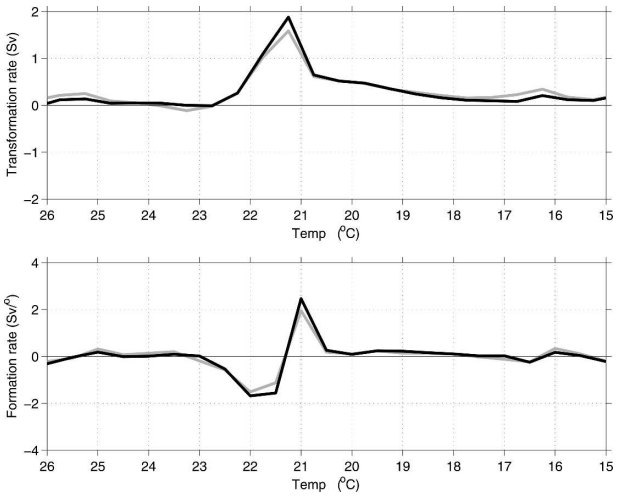

FIG. 11. (top) Volume flow A across the isotherms (Sv) obtained performing the Walin analysis on one year of daily data using Eq. (8) (gray line) and taking into account only the air–sea heat flux in Eq. (8) (black line). Comparison shows that the contribution of the diffusive heat flux acting across the isotherms is small. (bottom) The corresponding formation rates estimated as $\partial A/\partial T$.

mode water (there is no peak at temperatures around 21°C). As it takes tens of days for the mode-one eddy to cross the computational domain—of some 10° of longitude—the results obtained from the monthly means are somewhat similar to those obtained using daily mean data, since monthly means resolve eddy filamentation.

The large difference in both the transformation and formation rate estimates based on synoptic (daily) and time-averaged (annually averaged) data indicates that formation rates implied by smooth climatological data, which do not resolve the eddy processes, are likely to be in error. It is therefore of crucial importance to work with synoptic data. This is in accord with DM97, who shows that, when evaluating time-mean subduction rates, a Lagrangian frame of reference is required that follows the meandering surface density outcrops together with an accounting of the area over which the water mass outcrops. Tandon and Zahariev (2001, appendix) also comment that in order to obtain reliable formation rate estimates it is necessary to resolve the isopycnal meanders of the control surface.

4. Transformed Eulerian-mean (TEM) formalism

To what extent can we rephrase Walin's watermass analysis formulation so that it might be used with coarse-grained estimates of outcrop windows and air–sea fluxes? Averaging results is a loss of information, which must be recovered somehow. A natural way forward is to adopt a "transformed Eulerian-mean" (TEM) perspective in which advection of a mean tracer distribution is accomplished by a residual-mean velocity, while residual (nonskew) eddy fluxes appear as

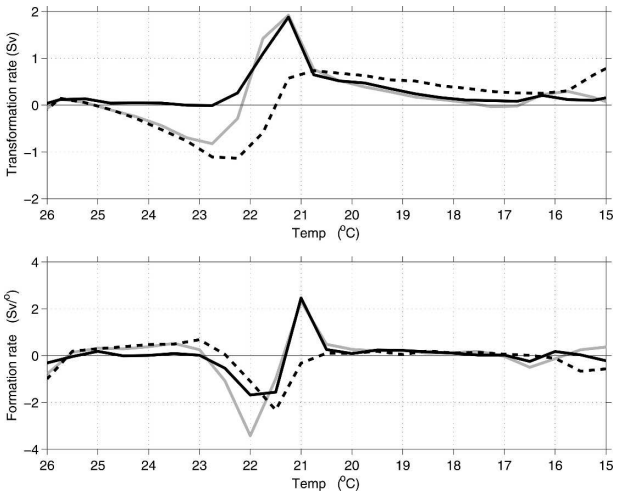

FIG. 12. Transformation rate obtained by neglecting diffusive heat flux acting across the isotherms, D, so Eq. (8) reduces to $A = F_{\text{air}-\text{sea}}$, ($A$; Sv) and formation rate obtained as $\partial A/\partial T$ using one year of data in the Walin analysis. The black solid line shows results obtained from analyzing daily data, the gray line shows results obtained using monthly temperature time averages to define both the outcrop windows as well as the air–sea heat flux (using Eq. 10), and the dashed line shows results obtained using the annually averaged temperature to define both the outcrop windows and the air–sea heat flux.

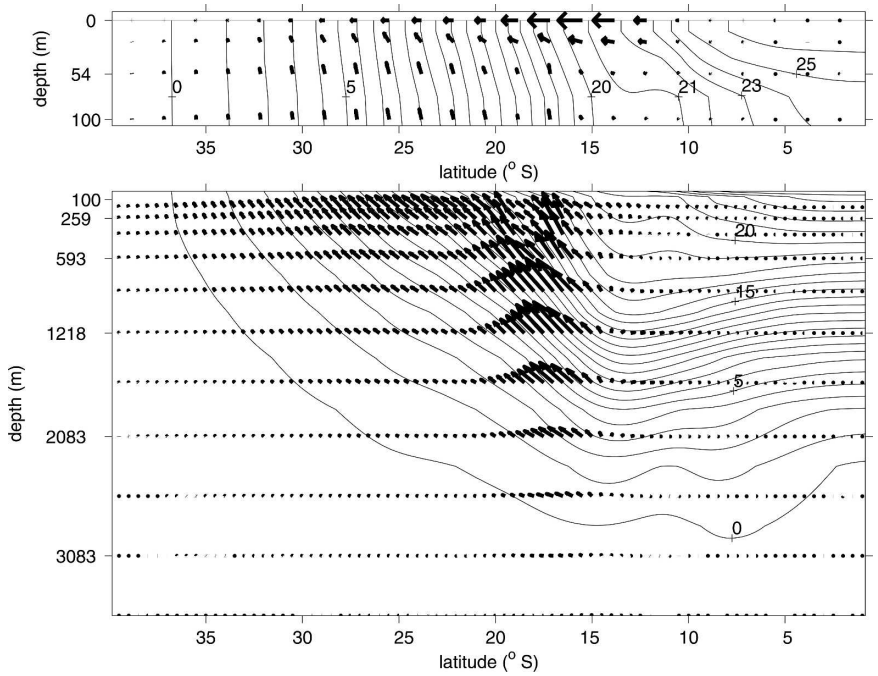

FIG. 13. Meridional cross section of zonally averaged mean isopycnals that coincide with the mean isotherms (solid line; °C) and zonally and time-averaged eddy temperature flux $\overline{\mathbf{u}'T'}$ (arrows). (top) The surface diabatic layer where the longest arrow corresponds to a flux of 0.15°C m s^{-1}. (bottom) The near-adiabatic interior, where the longest arrow corresponds to a flux of 0.02°C m s^{-1}. The light solid line indicates the surface.

forcing terms on the rhs. The residual flow is related to (in fact, in a quasigeostrophic and statistically steady state, is equal to) the mass-weighted mean circulation in isopycnal coordinates (Andrews et al. 1987). It is the sum of the "eddy induced"—also known as the "quasi Stokes"—flow and the Eulerian mean flow. The residual mean therefore yields the flow that transports mean tracer fields (such as heat, passive tracers, and active tracers such as potential vorticity) in an eddying ocean (see, e.g., DM97; Marshall and Radko 2003; Kuo et al. 2005).

Specifically, we write the time-mean of the buoyancy equation (5) in the form

$$\frac{\partial \overline{\sigma}}{\partial t} + \boldsymbol{\nabla} \cdot (\mathbf{u}_{\text{res}} \overline{\sigma} + \mathbf{N}_{\overline{\sigma}} + \mathbf{N}_{\sigma_{\mathbf{res}}}) = 0, \qquad (15)$$

where $\mathbf{u}_{\text{res}}$ is the residual flow and $\mathbf{N}_{\sigma_{\mathbf{res}}} = (\overline{\mathbf{u}'\sigma'} \cdot \mathbf{n}_\sigma)\, \mathbf{n}_\sigma$ is the "residual eddy flux"—the flux that is not "skew" (Plumb and Ferrari 2005). If $\overline{\mathbf{u}'\sigma'} \cdot \mathbf{n}_\sigma = 0$, then $\mathbf{N}_{\sigma_{\mathbf{res}}} = 0$ and the eddy flux divergence can be entirely represented as an advective process and subsumed into $\mathbf{u}_{\text{res}}$. Otherwise, there will always be a nonadvective contribution associated with the eddies. DM97 has pointed out that eddy buoyancy flux within the mixed layer includes both advective and diffusive components, where the latter are due to diabatic mixing along the sea surface. Therefore, the rate at which a water mass is subducted from the surface mixed layer into the ocean interior is determined by the air–sea buoyancy flux and the diapycnal component of eddy buoyancy forcing [cf. our Eqs. (15) and (16) with DM97 Eqs. (14)–(16)]. The contribution of the nonadvective component of eddy buoyancy flux has largely been neglected in previous studies. DM97 includes it when developing a theoretical framework for diagnosing the contribution of mesoscale eddies to the subduction of a water mass. However, when applying the theory to the Southern Ocean circulation, DM97 neglects the diffusive component of eddy buoyancy flux, given by $\overline{\mathbf{u}'T'} \cdot \mathbf{n}_T$, in the mixed layer. Marshall and Radko (2003) argue that the diffusive term is important in the Southern Ocean. What do we observe in our numerical simulation?

The zonal average temperature and eddy heat flux, Fig. 13, show that the "raw" eddy flux is parallel to the isotherms everywhere in the channel except in the vicinity of the main jet and in the surface diabatic layer, just as found in Kuo et al. (2005). Kuo et al. estimate the depth of the surface diabatic layer in the presence of the mixed layer as the sum of the mean mixed layer depth and the maximum thickness of the ventilated

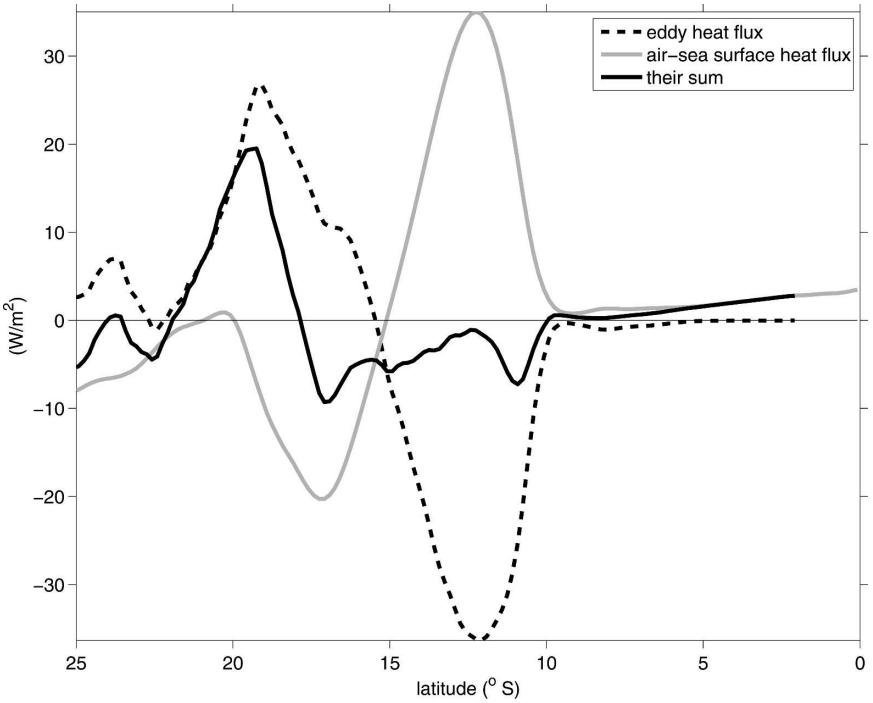

FIG. 14. Air–sea and eddy heat fluxes (W m^{-2}) zonally and time-averaged over a 100-yr period: divergence of the diapycnal component of eddy heat flux per unit area integrated over the mixed layer depth h, $\int_{-h}^{0} \nabla \cdot [\overline{\mathbf{u}'T'} \cdot \mathbf{n}_T]\, dz$ (dashed line), the air–sea surface heat flux H, given by Eq. (1) (gray line), and their sum (black line). The mixed layer depth is chosen to be 165 m (see Fig. 13, top). Positive flux corresponds to ocean gaining heat.

layer given by $\sqrt{\overline{T'^2}}/\overline{T_z}$, where $\sqrt{\overline{T'^2}}$ is the eddy temperature perturbation at the surface and $\overline{T_z}$ is the mean vertical temperature gradient at the base of the surface diabatic layer. We estimate that the depth of the surface diabatic layer is approximately 100 m in our calculation. Since the divergence of the diapycnal eddy heat flux is large in the surface layer (Fig. 13, top, shows a poleward eddy heat flux), it is evident that $N_{\sigma_{\text{res}}} \neq 0$; therefore Eq. (8) will have a contribution due to eddies:

$$D_{\text{eddy}} = \iint_{\text{diabatic zone}} \overline{\mathbf{u}'T'} \cdot \mathbf{n}_T \, d\mathcal{A}, \tag{16}$$

where the residual flux is integrated over the temperature surface as it cuts through the surface diabatic zone. Here $\mathbf{n}_T$ is a unit vector pointing outward normal to the isotherms. When diagnosing D_{eddy} we neglect the small-scale diffusive flux, which has already been shown to be very small (section 3c).

Figure 14 shows the zonally and time-averaged residual eddy heat flux integrated over the outcropping temperature surface in the mixed layer, along with the zonally and time-averaged surface air–sea heat flux, both obtained from 100 years of model output. We see that the two terms oppose one another over the whole latitude range. The residual heat flux is poleward in the latitude range 10°–15°S. The air–sea heat flux, on the other hand, is directed into the ocean in this latitude range. Moreover, the magnitude of the eddy heat flux slightly exceeds that of the air–sea heat flux. Inspection of local balances shown in Fig. 9 reveals that over most of the basin, the air–sea heat flux and the eddy-induced heat flux are of comparable magnitude but of the opposite sign. However, poleward of 14°S, in the region where the eddies are strong, eddy fluxes slightly exceed air–sea heat flux.

Figure 15 shows the results of a residual-mean Walin analysis performed on 100 years of annually averaged model temperature data and eddy fluxes $\overline{\mathbf{u}'T'}$. In the temperature range from 21° to 25°C, residual eddy fluxes give rise to negative transformation rates. In the temperature range 18.5° to 21°C the magnitude of heat loss due to air–sea interaction slightly exceeds lateral eddy transfer, inducing negative transformation rates. This results in the formation of 0.25 Sv °C^{-1} of 21°C water, which is much lower than the actual formation rate but now, at least, is of the correct sign. However, the considerable disconnect between the formation

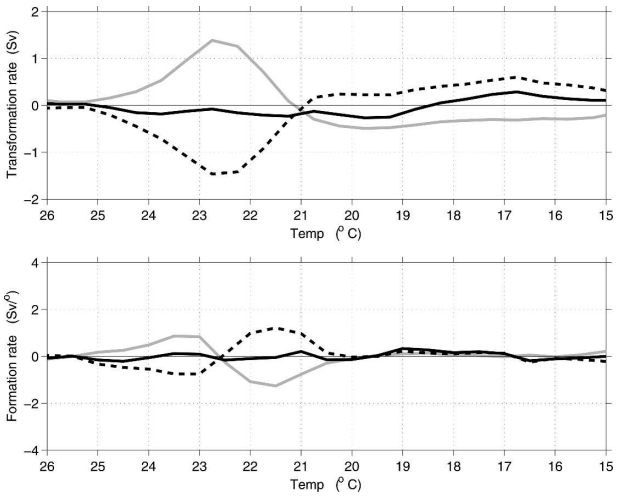

FIG. 15. (top) Volume flow across the isotherms A (Sv) obtained from the modified Walin analysis performed on 100 years of annually averaged model temperature data. The black line shows results based on the sum of vertically integrated (over 100 m) diapycnal eddy heat flux divergence and air–sea heat flux divergence, the gray line shows results from air–sea heat flux divergence, and the dashed line shows results from vertically integrated diapycnal eddy heat flux divergence. (bottom) The corresponding formation rates obtained as $\partial A/\partial T$, using the same plotting convention as in the top panel. Note the similarity between the gray line and the formation rate obtained from annually averaged data in Fig. 12, dashed line.

rates obtained here and those obtained using eddy-resolving data (Figs. 11 and 12) clearly indicates that it is necessary to follow the instantaneous isopycnals in order to accurately estimate formation rates (Garrett and Tandon 1997).

The formation rate calculated using the TEM framework is different from the formation rate calculated using daily data, primarily because the use of daily data provides sufficient resolution in time to be able to follow the isopycnals, so calculated formation rates are correctly assigned to the density interval where the formation occurs. When working in the TEM framework, on the other hand, the data have been averaged in time at a fixed position, so the calculated formation rates are estimated between the mean isopycnals. Since the isopycnals move around in space with time, formation that occurs in a certain density interval will inevitably become smeared over several neighboring density intervals.

5. Effect of strength of thermal coupling

How do our results depend on the magnitude of the air–sea coupling parameter? Cox (1985) and Böning and Budich (1992) showed that large-scale ocean circulation exhibits compensation between $\bar{\mathbf{u}} \cdot \boldsymbol{\nabla}\bar{T}$ and $\boldsymbol{\nabla} \cdot (\overline{\mathbf{u}'T'})$ in eddy-permitting numerical model simulations. Drijfhout and Walsteijn (1998) showed that the degree of compensation depends critically on the strength of the air–sea coupling and that the results of Cox (1985) and Böning and Budich (1992) may be a consequence of inadequate air–sea interaction, that is, too weak thermal coupling between the atmosphere and the ocean on the eddy scale.

Huang (1989) suggested that the strength of thermal driving can be expressed by the nondimensional parameter Γ, which is the ratio of the advection time and the relaxation time of the upper-layer temperature field toward surface air temperature:

$$\Gamma = L/(U\tau), \tag{17}$$

where L is a representative length scale, U is the advection velocity, and τ is the relaxation time scale. Thus, if Γ is small, diabatic effects are small relative to advective effects, and the air–sea coupling is weak. In this limit one might expect to observe compensation between mean and eddy heat transport, as discussed in Drijfhout (1994a,b). In the experiment reported here, the appropriate length scale is that of the eddy itself; eddy filaments are advected around the mode one eddy in approximately 10 days. Thus $L \approx 1000$ km (the distance over which eddies advect filaments), $U \approx 3$–4 m s^{-1} (a typical velocity by which filaments are advected), and $\tau = 30$ days, giving a $\Gamma \approx 0.13$ and suggesting that compensation ought, indeed, be observed in our experiment. Note, however, that we cannot directly compare our estimate with quoted values for Γ since the coupling depends on the details of the oceanic and atmospheric flow configuration (Drijfhout 1994b).

In ocean-only models, thermal coupling coefficients are tuned to match typical SST–air temperature anomalies at the scale of 1000 km. Drijfhout (1994b) has suggested that the thermal coupling at the eddy scale would undergo a transition between weak and strong coupling when the thermal coupling coefficient becomes larger than about 100 W m^{-2} K^{-1}. The thermal coupling coefficient appropriate to our calculation may be found by differentiating Eq. (1) wrt T to yield

$$\frac{\partial \mathcal{H}}{\partial T} = -\frac{\rho c_w d_1}{\tau}$$

or, inserting numbers, 13 W m^{-2} K^{-1} if $\tau = 30$ days (cooling if SST increases). This confirms that, with this relaxation time scale, our experiment is in the weak coupling limit: eddy filaments can be advected large meridional distances without significant change in temperature and so find themselves in regions where they are much warmer then the air above. Heat is thus lost

to the atmosphere, triggering convection and giving rise to subduction of low PV water.

To see what happens when coupling is stronger we reran the numerical simulation with a relaxation time of 6 days, which yields a Γ of about 0.7. The most important result is that the temperature of eddy filaments quickly becomes almost indistinct from that of the surrounding water. Moreover, with stronger coupling, the eddy field is smoother and there is considerably less filamentation (Fig. 13, top). The meridional distribution of sea surface temperature is more uniform, as is the air–sea heat flux. The strongest air–sea heat exchange is due to the effects of horizontal mixing and stirring caused by the mode one eddy, so the typical air–sea heat flux pattern shows the ocean gaining heat in the equatorward half of the mode one eddy and losing heat in the poleward half. This pattern is somewhat similar to time-averaged air–sea heat flux from the weak coupling case, but the instantaneous heat flux pattern shows less correlation with filaments than in the weaker coupling case.

The strong coupling transformation rate promotes ocean heat loss in the poleward half of the mode one eddy, transforming water over broader temperature ranges and larger surface outcrop areas, resulting in enhanced low-PV water formation rate [Fig. 16 (bottom), based on analysis of one year of daily data, shows that 4 Sv of water is formed.] This is in agreement with the results of Drijfhout (1994a) and of Drijfhout and Walsteijn (1998), who found that there is less compensation between eddy and mean flow transport in the case of strong coupling. Comparison of Figs. 5 and 16 (top panels) as well as Figs. 12 and Fig. 16 (bottom panels) confirms that water mass formation, a consequence of air–sea heat exchange, depends crucially on the strength of thermal coupling.

6. Discussion and conclusions

The effects of eddy modulation of air–sea interaction and convection on the process of mode water formation have been studied in a baroclinically unstable wind- and buoyancy-driven model flow in a pie-shaped sector of the sphere. The Walin (1982) analysis has been used to estimate formation rates in the presence of eddies and to characterize the role of eddies in that process. In an ideal world, water mass formation would be computed using synoptic outcrop fields and synoptic air–sea fluxes (Garrett and Tandon 1997; DM97). We therefore first performed Walin's analysis using model data with sufficient resolution in space and time to capture the eddies. The result (Fig. 11) shows a pronounced peak in the formation rate in the appropriate temperature range, corresponding to that of the water that feeds the low-PV pool (see Fig. 6). However, when formation rates are estimated from temperature and heat flux data that have been averaged in time at a fixed location, they yield erroneous formation rates. The large difference between the formation rate estimates, obtained from synoptic data that resolve the eddies and time-averaged data that do not resolve them, point to the fundamental importance of including eddy effects in the analysis. The considerable disconnect between the formation rates obtained here and the ones obtained using eddy-resolving data (Figs. 11 and 12) clearly indicates that it is necessary to follow the instantaneous isopycnals in order to accurately estimate formation rates (Garrett and Tandon 1997). Diagnosis within a TEM framework improves our estimates and provides a theoretical framework, but is not quantitatively useful.

In our numerical simulation, residual eddy heat fluxes and air–sea fluxes are found to play a comparable role in setting the transformation. They are of the opposite sign and nearly cancel each other. A heat budget rephrased in terms of TEM shows that this is to be expected if the residual circulation is weak, as in the flow analyzed here. In our calculation the eddy-induced mean flow tends to balance the Eulerian-mean flow over most of the basin. Because of this near cancellation, water mass formation estimates based on nonsynoptic air–sea heat flux data and outcrops may "miss" one of the two dominant heat transfer mechanisms and, hence, yield formation rates that are very much in error, as summarized in the following modified Walin balance:

$$A_{\mathrm{res}} = \underbrace{A_{\mathrm{mean}} + A_{\mathrm{eddy}}}_{\text{partial cancellation}} = \underbrace{F_{\text{air-sea}} - \frac{\partial D_{\mathrm{eddy}}}{\partial \sigma}}_{\text{partial cancellation}} \quad (18)$$

Note that eddy terms appear on both sides of the equation. The diapycnal volume flux in a turbulent ocean has a contribution from the eddy-induced transport A_{eddy}, which, as in the calculations presented here, largely cancels A_{mean}. This is certainly true in strong frontal regions such as the Antarctic Circumpolar Current. For example, the vanishing of the "Deacon cell" in the Southern Ocean is a case in point, where equatorward Ekman transport is largely balanced by poleward eddy-induced transport (see, e.g., Danabasoglu et al. 1994; Doos and Webb 1994; McIntosh and McDougall 1996; Karsten and Marshall 2002). So, not only may $\partial D_{\mathrm{eddy}}/\partial\sigma$ partially cancel $F_{\mathrm{air-sea}}$, but also A_{mean} and A_{eddy} tend to compensate one another. In the conventional application of air–sea flux analyses to watermass

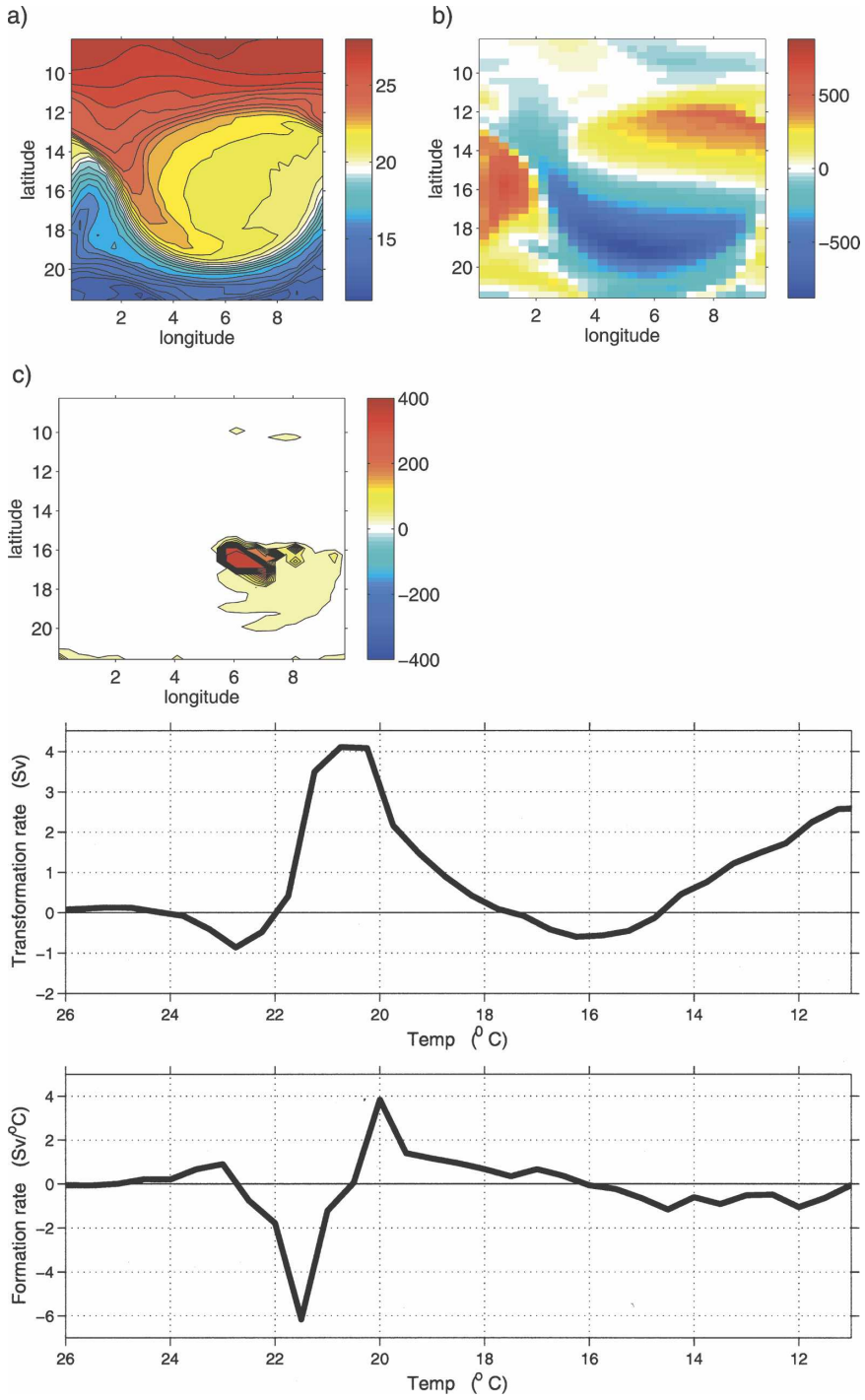

FIG. 16. Results from a numerical experiment in which strong thermal coupling was employed (relaxation time of 6 days). (top) Synoptic maps of (a) SST with contour interval 0.5°C, (b) heat flux (W m^{-2}), and (c) mixing layer depth with contour interval 25 m. (bottom) Transformation rate obtained from $A = F_{\text{air}-\text{sea}}$, ($A$; Sv) and formation rate using 1 year of daily air sea heat flux data and daily estimates of outcrop windows in the Walin analysis.

formation estimates—as in, for example, Speer and Tziperman (1992)—A_{mean} is set equal to $F_{\text{air}-\text{sea}}$, resulting in a likely erroneous estimate of formation rates in the vicinity of fronts, where D_{eddy} and A_{eddy} are important.

In the experiments presented here, mode water is formed when near-surface water parcels are displaced large meridional distances in filamentary structures associated with the eddies. Large air–sea temperature differences, and hence vigorous air–sea interaction, are induced that triggers convection and the creation of low potential vorticity water. Because of the simple geometry adopted in our model, eddy processes are the only mechanism at work driving disequilibrium between the atmosphere and the ocean. In the ocean, however, water is also displaced from its equilibrium latitude by the mean flow, in western boundary currents and jets, a process that is absent from our model. Additionally, synoptic variability of the atmosphere and seasonal cycle are both key processes in STMW formation but absent in our model. Therefore, in a system like the Gulf Stream mode water can also be formed in the absence of eddies. Indeed, coarse-resolution models show mode water formation (e.g., Hazeleger and Drijfhout 1998, 1999; Marsh and New 1996; Paiva and Chassignet 2002). It remains to be seen whether the role of eddies in mode water formation explored here is a true reflection of the role played by eddies in nature.

Acknowledgments. IC acknowledges support from NSF, under Grant OCE-0426307. Author IC thanks Leif Thomas for motivating discussions and insightful comments and two anonymous reviewers for suggesting significant improvements to the text. Author JM was supported by an NSF OCE grant supporting the CLIMODE project.

REFERENCES

Andrews, D. G., J. R. Holton, and C. B. Loevy, 1987: *Middle Atmosphere Dynamics.* Academic Press, 489 pp.

Böning, C. W., and R. G. Budich, 1992: Eddy dynamics in a primitive equation model: Sensitivity to horizontal resolution and friction. *J. Phys. Oceanogr.,* **22,** 361–381.

Cox, M. D., 1985: An eddy resolving numerical model of the ventilated thermocline. *J. Phys. Oceanogr.,* **15,** 1312–1324.

Danabasoglu, G., J. C. Mc Williams, and P. R. Gent, 1994: The role of mesoscale tracer transport in the global ocean circulation. *Science,* **264,** 1123–1126.

Dewar, W. K., 1986: On the potential vorticity structure of weakly ventilated isopycnals: A theory of subtropical mode water maintenance. *J. Phys. Oceanogr.,* **16,** 1204–1216.

Dong, S., and K. A. Kelly, 2004: Heat budget in the Gulf Stream region: The importance of heat storage and advection. *J. Geophys. Res.,* **99,** 18 481–18 499.

Donners, J., S. S. Drijfhout, and W. Hazeleger, 2005: Water mass transformation and subduction in the North Atlantic. *J. Phys. Oceanogr.,* **35,** 1841–1860.

Doos, K., and D. J. Webb, 1994: The Deacon cell and other meridional cells of the Southern Ocean. *J. Phys. Oceanogr.,* **24,** 429–442.

Drijfhout, S. S., 1994a: Heat transport by mesoscale eddies in an ocean circulation model. *J. Phys. Oceanogr.,* **24,** 353–369.

——, 1994b: Sensitivity of eddy-induced heat transport to diabatic forcing. *J. Geophys. Res,* **99,** 18 481–18 499.

——, and F. H. Walsteijn, 1998: Eddy-induced heat transport in a coupled ocean–atmosphere anomaly model. *J. Phys. Oceanogr.,* **28,** 250–265.

Ebbesmeyer, C. C., and E. J. Lindstrom, 1986: Structure and origin of 18° Water observed during the POLYMODE Local Dynamics Experiment. *J. Phys. Oceanogr.,* **16,** 443–453.

Garrett, C., and A. Tandon, 1997: The effects on water mass formation of surface mixed layer time-dependence and entrainment fluxes. *Deep-Sea Res.,* **44,** 1991–2006.

——, K. Speer, and E. Tragou, 1995: The relationship between water mass formation and the surface buoyancy flux, with application to Phillips' Red Sea model. *J. Phys. Oceanogr.,* **25,** 1696–1705.

Hanawa, K., and L. D. Talley, 2001: Mode waters. *Ocean Circulation and Climate,* G. Siedler and J. Church, Eds., International Geophysics Series, Vol. 77, Academic Press, 373–386.

Hazeleger, W., and S. S. Drijfhout, 1998: Mode water variability in a model of the subtropical gyre: Response to anomalous forcing. *J. Phys. Oceanogr.,* **28,** 266–288.

——, and ——, 1999: Stochastically forced mode water variability. *J. Phys. Oceanogr.,* **29,** 1772–1786.

——, and ——, 2000: Eddy subduction in a model of the subtropical gyre. *J. Phys. Oceanogr.,* **30,** 677–695.

Huang, R. X., 1989: Sensitivity of a multilayered oceanic general circulation model to the sea surface thermal boundary condition. *J. Geophys. Res.,* **94,** 18 011–18 021.

Jenkins, W. J., 1982: On the climate of a subtropical ocean gyre: Decade timescale variations in water mass renewal in the Sargasso Sea. *J. Mar. Res.,* **40** (Suppl.), 265–290.

Karsten, R., and J. Marshall, 2002: Constructing the residual circulation of the Antarctic Circumpolar Current from observations. *J. Phys. Oceanogr.,* **32,** 3315–3327.

Kelly, K. A., 2004: The relationship between oceanic heat transport and surface fluxes in the western North Pacific: 1970–2000. *J. Climate,* **17,** 573–588.

Klinger, B. A., J. Marshall, and U. Send, 1996: Representation and parameterization of deep convective plumes by mixing. *J. Geophys. Res.,* **101,** 18 175–18 182.

Kuo, A., R. A. Plumb, and J. Marshall, 2005: Transformed Eulerian-mean theory. Part II: Potential vorticity homogenization, and the equilibrium of a wind- and buoyancy-driven zonal flow. *J. Phys. Oceanogr.,* **35,** 175–187.

Kwon, Y.-O., and S. C. Riser, 2005: The general circulation of the western subtropical North Atlantic observed by using profiling floats. *J. Geophys. Res.,* **110,** C10012, doi:10.1029/2005JC002909.

Large, W. G., J. C. McWilliams, and S. C. Doney, 1994: Oceanic vertical mixing: A review and a model with a nonlocal boundary layer parameterization. *Rev. Geophys.,* **32,** 363–403.

Marsh, R., and A. L. New, 1996: Modeling 18° Water variability. *J. Phys. Oceanogr.,* **26,** 1059–1080.

Marshall, D., 1997: Subduction of water masses in an eddying ocean. *J. Mar. Res.,* **55,** 201–222.

Marshall, J., and T. Radko, 2003: Residual-mean solutions for the Antarctic Circumpolar Current and its associated overturning circulation. *J. Phys. Oceanogr.,* **33,** 2341–2354.

——, D. Jamous, and J. Nilsson, 1999: Reconciling "thermodynamic" and "dynamic" methods of computation of water-mass transformation rates. *Deep-Sea Res. I,* **46,** 545–572.

——, C. Hill, L. Perleman, and A. Adcroft, 1997a: Hydrostatic, quasi-hydrostatic, and non hydrostatic ocean modeling. *J. Geophys. Res.,* **102,** 5733–5752.

——, A. Adcroft, C. Hill, L. Perleman, and C. Heisy, 1997b: A finite volume, incompressible Navier–Stokes model for studies of the ocean on parallel computers. *J. Geophys. Res.,* **102,** 5753–5766.

McCartney, M. S., 1982: The subtropical recirculation of mode waters. *J. Mar. Res.,* **40** (Suppl.), 427–464.

McIntosh, P. C., and T. J. McDougall, 1996: Isopycnal averaging and the residual mean circulation. *J. Phys. Oceanogr.,* **26,** 1655–1660.

Paiva, A. M., and E. P. Chassignet, 2002: North Atlantic modeling of low-frequency variability in mode water formation. *J. Phys. Oceanogr.,* **32,** 2666–2680.

Panetta, R. L., 1993: Zonal jets in wide baroclinically unstable regions: Persistence and scale selection. *J. Atmos. Sci.,* **50,** 2073–2106.

Plumb, R. A., and R. Ferrari, 2005: Transformed Eulerian-mean theory. Part I: Nonquasigeostrophic theory for eddies on a zonal-mean flow. *J. Phys. Oceanogr.,* **35,** 165–174.

Rhines, P. B., 1994: Jets. *Chaos,* **4,** 313–341.

Schroeder, E. H., H. Stommel, D. W. Menzel, and W. J. Sutcliffe, 1959: Climate stability of eighteen degree water at Bermuda. *J. Geophys. Res.,* **64,** 363–366.

Speer, K., and E. Tziperman, 1992: Rates of water mass formation in the North Atlantic. *J. Phys. Oceanogr.,* **22,** 93–104.

Stommel, H. M., 1979: Determination of water mass properties of water pumped down from the Ekman layer to the geostrophyc flow. *Proc. Natl. Acad. Sci. USA,* **76,** 3051–3055.

Talley, L. D., and M. E. Raymer, 1982: Eighteen degree water variability. *J. Mar. Res.,* **40** (Suppl.), 725–775.

Tandon, A., and K. Zahariev, 2001: Quantifying the role of mixed layer entrainment for water mass transformation in the North Atlantic. *J. Phys. Oceanogr.,* **31,** 1120–1131.

Walin, G., 1982: On the relation between sea-surface heat flow and thermal circulation in the ocean. *Tellus,* **34,** 187–195.

Worthington, L. V., 1959: The 18° Water in Sargasso Sea. *Deep-Sea Res.,* **5,** 297–305.

——, 1976: *On the North Atlantic Circulation*. John Hopkins Oceanographic Studies, Vol. 6, The Johns Hopkins University Press, 110 pp.